

Magnesium Loss in Nd:YAG Pulsed Laser Welding of Aluminum Alloys



Z. MALEKSHAHI BEIRANVAND, F. MALEK GHAINI, H. NAFFAKH-MOOSAVY, M. SHEIKHI, and M.J. TORKAMANY

In the current investigation, the loss of magnesium (Mg) in Nd:YAG pulsed laser welding of a number of aluminum (Al) alloys was studied both experimentally and numerically. The experimental results showed that at a fixed average laser power, with the increasing pulse frequency, Mg concentration of the weld metals decreased. A numerical model was developed for the calculation of Mg evaporation from the weld pool. The model predicted a trend in the changes of Mg concentration of the weld pool, working best for alloys containing the higher levels of Mg. The calculations showed that with the increasing pulse frequency from 15 to 40 Hz, due to a decrease in the average temperature of the weld pool, Mg loss in terms of mass per unit area of the weld spot actually decreased from 230×10^{-5} to 120×10^{-5} kg/m². However, due to a decrease in the weld penetration/volume, the effective Mg loss of the weld metal in terms of concentration increased from 110×10^{-1} to 260×10^{-1} kg/m³. It was shown that due to interactions between Mg and other main alloying elements, the activity coefficient of Mg had to be modified for the model to accurately predict Mg evaporation of the weld pool.

<https://doi.org/10.1007/s11663-018-1315-7>

© The Minerals, Metals & Materials Society and ASM International 2018

I. INTRODUCTION

PULSE laser welding is now considered a favorable process to be applied to Al alloys due to advantages, including high heat intensity and low heat input. The presence of Mg in Al alloys increases strength through solid solution strengthening; the presence of both Mg and silicon produces a compound of Mg-silicide (Mg₂Si). In addition to strength, the resistance of the weld metal to solidification cracking is affected by Mg content.^[1] Michaud *et al.* measured the effect of base metal composition on solidification cracking in pulsed laser welding of Al-Cu alloys.^[2] The loss of alloying elements can also result in significant changes in the microstructure and degradation of mechanical properties of the weld.^[3–5] Vapor pressures of Al and Mg at 1473 K were 2 Pa and 2.5×10^5 Pa, respectively.^[6] It is reported that the temperature of the weld pool in pulsed laser welding can reach 2273 K and Mg is evaporated

both in conduction and keyhole modes.^[6,7] However, a higher level of Mg evaporation during keyhole mode is also reported.^[8] Tenner *et al.* developed an experimental and numerical model for measuring the density of metal vapor and pressure inside the keyhole during laser welding.^[9] The evaporation rate of volatile elements was mainly controlled by equilibrium between vapor pressure and temperature.^[6,10–12] Hence, in this respect, it is essential to estimate the surface temperature of the melt pool.^[6] However, there are other factors such as temperature distribution profile, chemical composition, and weld surface area that can affect the evaporation rate.^[13] By means of computed temperatures, mass loss, due to the vaporization of alloying elements, has been calculated.^[4] In another research, the physical processes influencing the changes in chemical composition due to the evaporation in the weld seam during laser beam welding were analyzed.^[14] Langmuir presented a simple equation to calculate vaporization of a pure metal in a vacuum; this approach has been employed to estimate the vaporization fluxes of alloying elements.^[6,15,16] Block-Bolten and Eagar calculated the evaporation rate of alloying elements in GTA welding of Al alloys using Langmuir equation. Likewise, Collur *et al.* studied the evaporation mechanisms of alloying elements during laser welding in the conduction mode.^[17] It was shown that Mg evaporation could occur in both continuous and pulsed Nd:YAG laser welding of 5086 and 5456 Al alloys, and that the amount of Mg loss in weld metal was affected by welding parameters.^[7] In other

Z. MALEKSHAHI BEIRANVAND, F. MALEK GHAINI, and H. NAFFAKH-MOOSAVY are with the Department of Materials Engineering, Tarbiat Modares University, Tehran 14115-143, Iran. Contact e-mail: fmalek@modares.ac.ir M. SHEIKHI is with the Department of Materials Engineering, Bu-Ali Sina University, Hamedan 65178-38695, Iran. M.J. TORKAMANY is with the Iranian National Center for Laser Science and Technology (INLC), Tehran 14665-576, Iran.

Manuscript submitted December 4, 2017.

Article published online June 25, 2018.

researches, it was established that Mg evaporation was minimized in a continuous mode^[16] and Mg loss increased linearly with the increasing pulse duration.^[18] In the current study, an attempt is made to further develop the previously suggested models for the evaporation of alloying elements in fusion welding and to take into account the nature of thermal cycles and consecutive melting in a pulsed laser process. A medium power Nd:YAG pulsed laser is used to autogenously weld four Al alloys which contain various concentrations of Mg.

II. METHOD

A. Theory

Figure 1(a) through (c) illustrates the sequence of events in a single pulse laser radiation and the process of the evaporation of Mg from the weld pool. The Mg mass in the original base metal in the volume to be melted was w_0 (kg); after irradiation with laser it changed to w_1 (kg).

Mg vapor outward flux “ J ” (kg/m² s) from the melt pool of Al-Mg alloy can be related to the absolute temperature of the melt pool (T) as follows^[7,15,19]:

$$J = \frac{0.583 \times \left(\frac{M}{T}\right)^{0.5} \times \gamma_{Mg} \times P_{Mg} \times X_{Mg}}{7.5}, \quad [1]$$

where P_{Mg} is the Mg vapor pressure in the molten weld metal, M is the Mg atomic weight (24×10^{-3} kg), γ_{Mg} is the Mg activity coefficient, X_{Mg} is the Mg molar fraction and T is the temperature. The factor 7.5 was used to account for the fact that the evaporation rate at one atmosphere pressure was less

than the evaporation rate in vacuum, based on previous experimental results. This factor was an empirical fit to make the equation work.^[15]

The vapor pressure of P_{Mg} metal at the temperature of T (K) can be expressed by the following equation^[7]:

$$\log P_{Mg} = \left(\frac{-7550}{T}\right) - (1.41 \times \log T) + 12.79. \quad [2]$$

X_{Mg} can be expanded as a function of Mg weight (w) or $X_{Mg} = f(w)$.^[20] Knowing the vapor flux of Mg, the Mg weight loss (w) at any pulse radiation (LOM) can be calculated as a function of surface area of the weld pool, A_s , and the pulse duration, t_p , by

$$\text{LOM} = k \times f(w), \quad [3]$$

where

$$k = \frac{t_p \times A_s \times 0.583 \times \left(\frac{M}{T}\right)^{0.5} \times \gamma_{Mg} \times P_{Mg}}{7.5}. \quad [4]$$

By dividing the mass of Mg evaporated (LOM) over the mass of the weld pool, the reduction in Mg concentration (C) is obtained. In Eq. [3], it is assumed that evaporation occurs only during laser radiation since the cooling time to complete solidification is negligible compared with t_p .^[21] The above equation is for a single pulse process, and it should be modified in order to be applicable to multiple pulsed laser processes having overlaps.

Overlapping factor (O_f) in pulsed laser welding can be obtained through the following equation^[22]:

$$O_f = \left[1 - \frac{R/f}{d_s + Rt_p}\right], \quad [5]$$

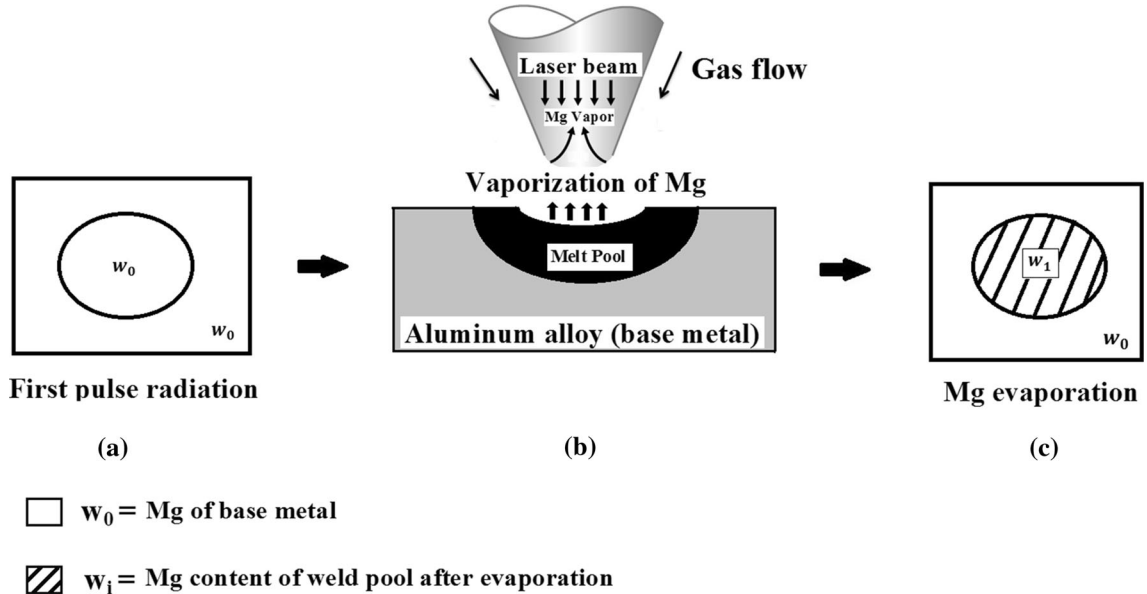


Fig. 1—Schematic illustration of events with regard to changes in Mg content as a result of radiation of a single pulse of laser. (a) The base metal with the Mg content (mass) of w_0 in the volume to be melted, (b) laser radiation and Mg evaporation from the melt pool surface, and (c) solidification of the weld bead with w_1 Mg content.

where R , f , d_s , and t_p are travel speed, frequency, spot diameter, and pulse duration, respectively (see Figure 2). The geometrical parameters shown in Figures 2 and 3(a) indicated that the contribution of the first weld spot in the second weld pool would be in the order of O_f^2 . At high overlapping factors, a point would experience multiple melting events.

In order to simplify the situation, two stages can be considered with regard to the Mg content of a point in the weld track:

1. Just melting and dilution due to mixing with the previous weld spot; In this stage, a weld pool with w'_i Mg mass, is formed (i represents the spot number). This stage is shown in Figure 3(b).

$$w'_i = (O_f^2 \times w_{i-1}) + ((1 - O_f^2) \times w_0). \quad [6]$$

2. Mg evaporation that changes the Mg content of the weld pool from w'_i to w_i .

$$w_i = w'_i - k \cdot f(w'_i). \quad [7]$$

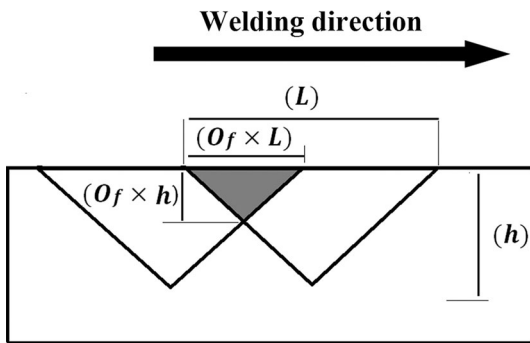


Fig. 2—Schematic illustration of overlapping indicating that the ratio of the metal from the previous weld pool forming on the second weld pool is in the order of O_f^2 .

With regard to Eqs. [2], [4], and [7], pulse duration, surface area of the melt pool, and the temperature of the weld pool are key factors governing k , the weight of the evaporated Mg (LOM), and in turn Mg weight of the weld pool after evaporation (w_i). With the increasing temperature, t_p and A_s , k and LOM increased, and consequently w_i decreased.

The Mg content of a point is a function of the number of pulses (n) that a point may experience; “ n ” is related to the travel speed (R), pulse frequency (f), and spot diameter (d_s) according to the following equation:

$$n = \frac{(d_s \times f)}{R}, \quad [8]$$

After the iteration of the above computations for $i = 1$ to n , the resultant w_n represents the Mg weight in the weld spot; accordingly, the final Mg concentration can be calculated if the size of the weld pool is known.

B. Numerical Modeling

A finite element model of the welding process is used to calculate the effect of process parameters on the weld pool temperature. For simulation, an axisymmetric three-dimensional model with the plane of symmetry, assuming free heat convections and radiations at all external surfaces except top surface and supposing forced convections and radiations at top surface, ignoring the melt flow in the weld pool, was considered and a half part of the weld metal was modeled.^[2,23–26] A relatively finer mesh size was used within the fusion zone, while a larger mesh size was used outside this zone. To establish the relative suitability of the mesh sizes, a mesh size dependency test was performed using ABAQUS simulations. When 10^{-5} -m mesh size was set for fusion zone, the differences among temperatures were found to be negligible for the purpose of this study; the thermal history was also found to be the same. The mesh

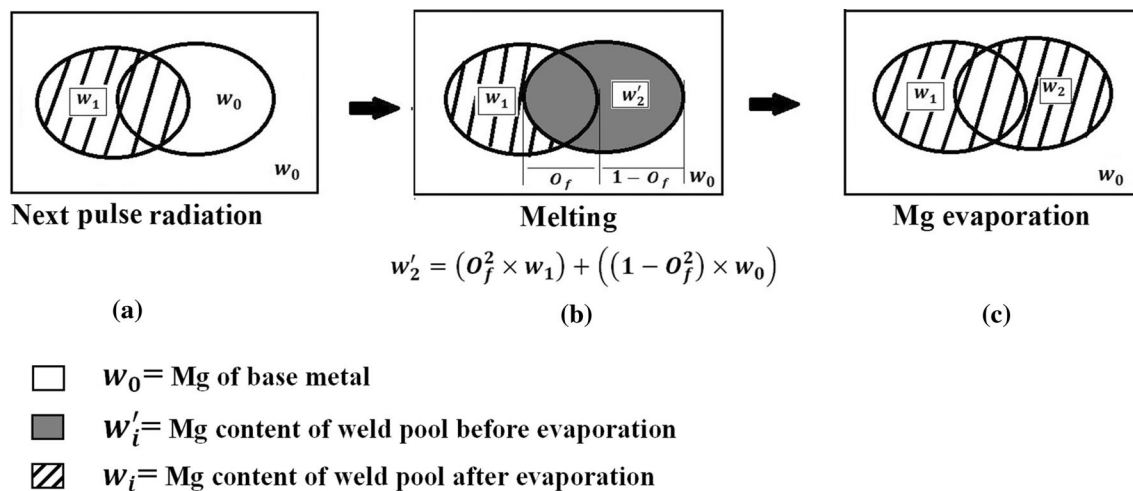


Fig. 3—Schematic illustration of different steps in the Mg content changes within the second laser pulse. (a) First weld spot is solidified, (b) second weld pool is formed and Mg evaporation occurs, and (c) the second weld spot is solidified.

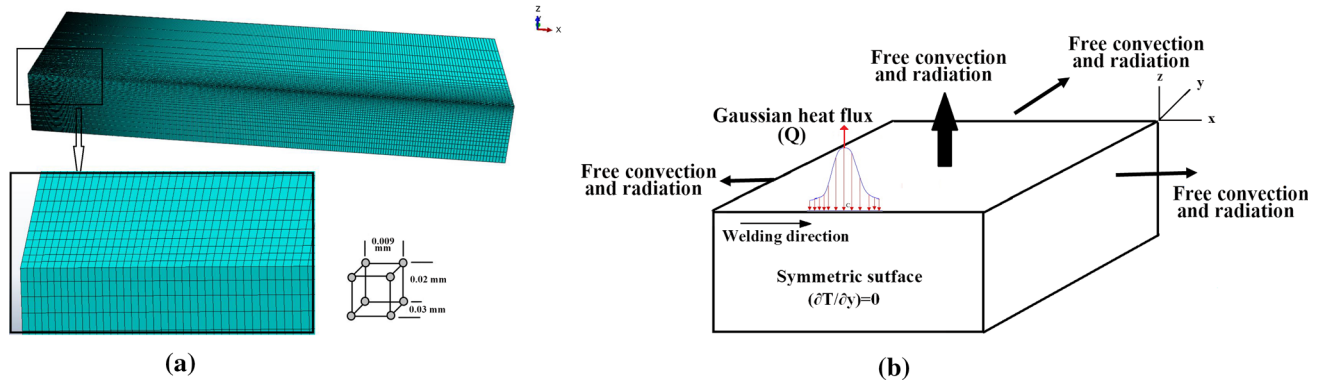


Fig. 4—(a) Mesh details, (b) schematic of surface heat flux and boundary conditions applied in the numerical modeling of laser welding process.

Table I. Material Properties Used in the Calculations of the Weld Pool Temperature^[27,28]

Properties	2024 Alloy	6061 Alloy	5083 Alloy	5454 Alloy
Heat transfer coefficient on top surface (W/m ² K)	20	20	20	20
Heat transfer coefficient on other surfaces (W/m ² K)	5	5	5	5
Thermal conductivity at 25 °C (W/mK)	151	154	117	134
Specified heat capacity of solid (J/kg K)	875	896	924	900
Specified heat capacity of liquid (J/kg K)	1273	1230	1261	1340
Density of solid (kg/m ³)	2780	2700	2670	2070
Density of liquid (kg/m ³)	2375	2240	2550	2010
Solidus temperature K (°C)	775 (502)	855 (582)	848 (575)	875 (602)
Liquidus temperature K (°C)	911 (638)	925 (652)	911 (638)	919 (646)
Modulus of elasticity at 298 K (25 °C) (N/m ²)	73.1 × 10 ⁻³	68.9 × 10 ⁻³	72 × 10 ⁻³	69.6 × 10 ⁻³
Thermal expansion at 298 K (25 °C) (1/K)	22.9 × 10 ⁻⁶	22 × 10 ⁻⁶	24 × 10 ⁻⁶	23.7 × 10 ⁻⁶

details are shown in Figure 4(a). A schematic of the heat source application and the applied thermal boundary conditions are shown in Figure 4(b).

The governing equation of heat transfer is

$$\left[\frac{\partial^2 T}{\partial x^2} \right] + \left[\frac{\partial^2 T}{\partial y^2} \right] + \left[\frac{\partial^2 T}{\partial z^2} \right] = \frac{\rho c_p}{k} \frac{\partial T}{\partial t}, \quad [9]$$

where C_p and k are heat capacity and heat conductivity coefficients, respectively. Room temperature, 298 K (25 °C), was considered as the initial temperature of the sample. Laser radiation was simulated by applying surface heat flux distribution to the top surface of the sample. Solution to this problem was provided by means of ABAQUS software, and the surface heat flux was defined *via* Dflux subroutine in the FORTRAN programming language. In this subroutine, a two-dimensional equation of heat flux is used with Gaussian distribution in terms of time and location in laser welding in the conduction mode. The final equation is^[27]

$$Q = \frac{6P\eta_v\sqrt{3}}{a_1a_2\pi\sqrt{\pi}} e^{\left[\left(\frac{-3}{a_1^2+a_2^2} \right) * [y^2 + [x-x_0-vt]^2] \right]}. \quad [10]$$

In the above equation, x_0 , v , y , and t are the overlapping factor, the travel speed of the laser beam, the location of the laser beam, and the time of welding, respectively^[19]; a_1 and a_2 represent dimensions of the welding pool ($a_1 = a_2 = 0.35$ mm actual). P is average power of the laser beam, and η_v is the absorption coefficient of the laser beam. The absorption coefficient was taken as 0.36.^[19] The parameters used in the calculations are shown in Table I. Among these material properties, specific heat, density, thermal conductivity, and modulus of elasticity were considered temperature dependent. Also emissivity, Poisson ratio, and Stefan-Boltzman constant were considered as 0.022, 0.33, and 5.67 J/K² m⁴, respectively.^[26,28]

C. Experiments

Sheets of Al alloys (2×10^{-3} m thick) with chemical compositions shown in Table II were used for making the weld runs. A pulsed Nd:YAG laser machine, IQL-10 model with an optical lens (75×10^{-3} m focal length), was used for welding. This laser source is able to produce combinations of pulse durations and frequencies from 2×10^{-4} to 2×10^{-2} seconds and 1 to 1000 Hz, respectively, but it is limited to an average power of 400 W. The shielding gas was argon at a flow

Table II. Chemical Composition of the Aluminum Alloys (Wt Pct)

Aluminum Alloy	Si	Fe	Cu	Mn	Mg	Cr	Zn	Ti
6061-T4	0.59	0.31	0.2	0.15	0.75	0.19	0.003	0.02
2024-T851	0.16	0.3	4.3	0.61	1.45	0.05	0.08	0.05
5454-O	0.1	0.3	0.07	0.79	3.04	0.1	trace	0.01
5083-H321	0.15	0.15	0.01	0.72	4.3	0.06	trace	0.01

Table III. Pulsed Laser Welding Process Parameters Used in Making Weld Runs

Test Run Identification Number	2	3	4	5
Laser pulse frequency (Hz)	15	20	25	40
Pulse energy (J)	13.3	10	8	5
Pulse duration (s)	0.007	0.006	0.005	0.004
Peak power (K W)	1.9	1.6	1.6	1.25
Duty cycle (pct)	10.5	12	12.5	16
Overlap factor (pct)	55	65	72	82
Travel speed (m/s)	0.005	0.005	0.005	0.005
Average power (W)	200	200	200	200
Heat input (J/m)	40000	40000	40000	40000

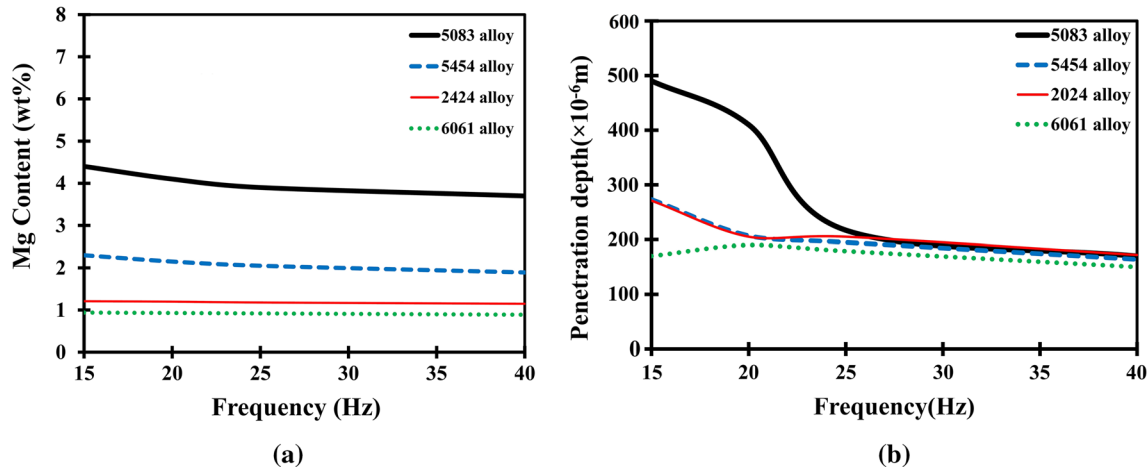


Fig. 5—Changes in the Mg content and weld penetrations as a function of laser pulse frequency. (a) Mg content of weld metals, (b) weld penetrations.

rate of 10 liters per minute. The power meter 5000W-LP model was used for measuring the laser power. After some preliminary test runs, the laser parameters were selected such that all the experimental welds were in the conduction mode with the spot diameter, average power, and travel speed fixed at 7×10^{-4} m, 200 W, and 5×10^{-3} m/s, respectively.

Table III shows the laser weld process parameters used for making the test runs (autogenous/bead on plate). Transverse cross sections of the samples were prepared and weld profiles were studied with an optical microscope while the weld metal were analyzed using an Electron Probe Microanalyser (EPMA) SX100 model from CAMECA, to determine the variations observed in the Mg weight percent. It is worthwhile to mention that the initial tests for compositional measurements have

been performed using EDS analysis, but it was found not to be accurate enough for the purpose of this investigation. The area for chemical analysis using EPMA was set at 5×10^{-6} m \times 5×10^{-6} m. Three different points of each sample were examined and the average was determined.

III. RESULTS

A. Experiments

EPMA analysis of the chemical composition of the weld metals showed that alloying elements other than Mg did not significantly change with respect to those in the base metal. The Mg weight percent of the weld metal and the measured weld penetration corresponding to the

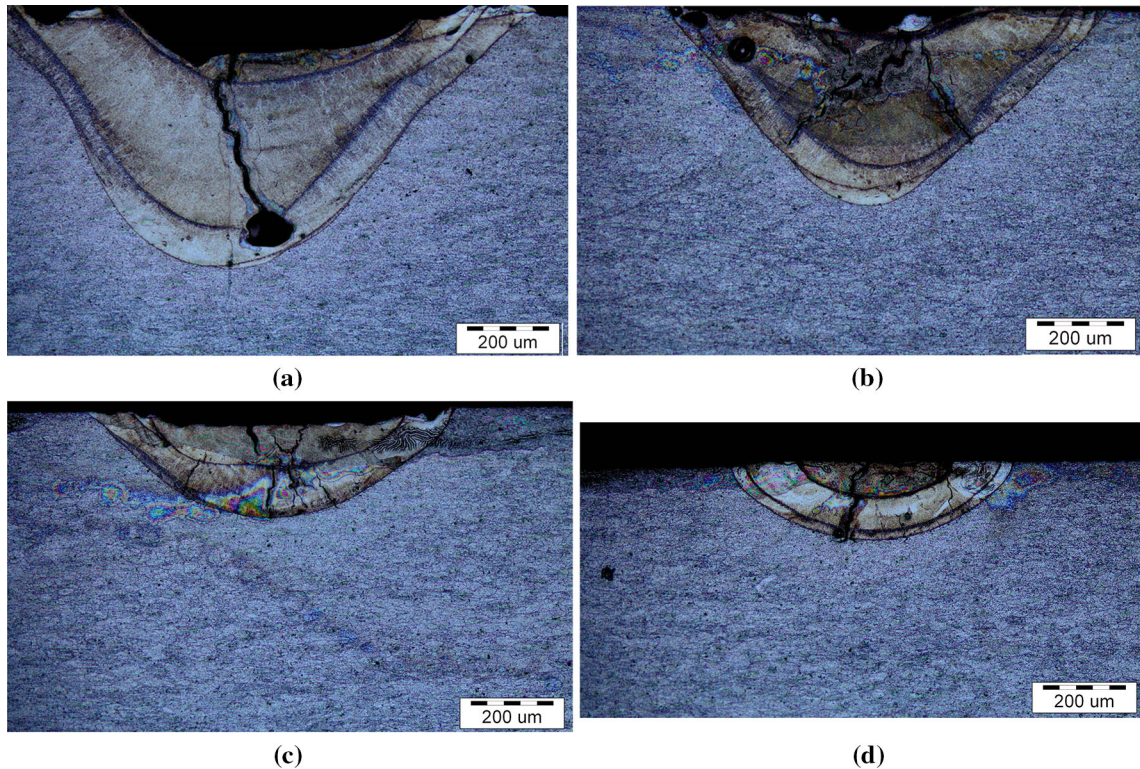


Fig. 6—Optical images of weld metals cross sections of 5083 alloy at various frequencies. (a) 15 Hz, (b) 20 Hz, (c) 25 Hz, and (d) 40 Hz.

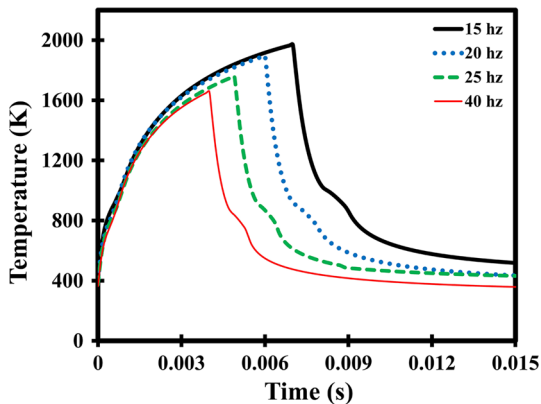


Fig. 7—The temperature history of the weld pool center as calculated for different laser pulse frequencies (average power fixed) for 2024 alloy.

four Al alloys welded at different frequencies are shown in Figure 5. It is seen that for Al alloys 5083 and 5454, the Mg content of the weld metals and the penetration of welds significantly decreased with the increasing pulse frequency. However, for 6061 and 2024 alloys, the variation of Mg and weld penetration were less evident.

Figure 6 corresponds to the cross section of the welds of 5083 Al alloy made at various laser pulse frequencies (at fixed average power and travel speed). It shows that with the increasing pulse frequency, the penetration (and the volume of the weld metal) decreased.

B. Simulation

The temperature of the weld pool was estimated by the simulation of the pulsed laser welding process. The calculations were performed for all four alloys (5083, 5454, 2024 and 6061 alloys) and the thermal cycle parameters were obtained. However, to save space, only the results of the calculation of the thermal cycle for 2024 alloy is shown here (see Figure 7). Subsequently, the validation of the simulation process (as explained later) was checked for 2024 alloy. The reason was that the available thermodynamic properties of the 2024 alloy were more comprehensive in comparison with other Al alloying elements under investigation in this study.

With reference to Figure 7, it is worthwhile to note that in the pulse laser welding, the heating rate was lower than the rate of cooling. This is due to the nature of the pulsing in the process (Turn on the pulse and turn it off) and the high thermal conductivity of aluminum alloys. This finding was consistent with the results obtained by other researchers. However, in continuous laser welding processes, the reverse phenomena is observed and the heating rate is much higher than the cooling rate.^[29,30]

The calculations predicted that the peak and average temperatures of the weld pool decreased with the increasing laser frequency. In order to assess the validity of the simulation results, the dimension of the actual weld pool was compared to that predicted by the numerical results (see Figure 8).

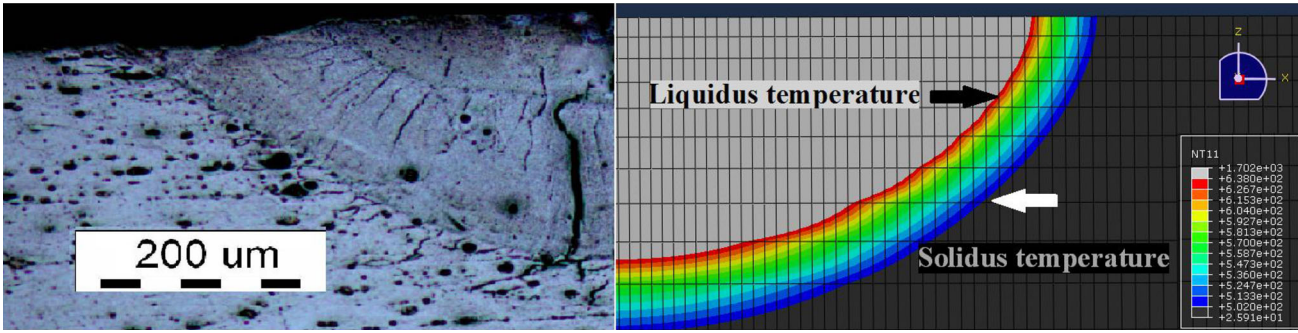


Fig. 8—Comparison of actual weld pool dimension to that obtained by simulation for 2024 alloy at the frequency of 15 Hz. Temperatures above liquidus temperature (638 °C) are shown in gray and temperatures below solidus temperature (502 °C) are shown in black.

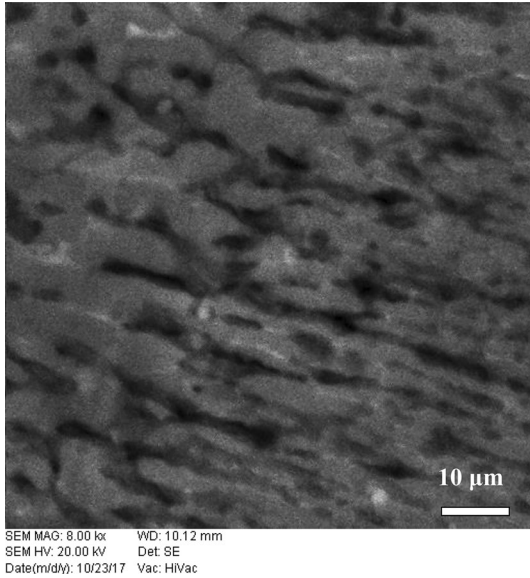


Fig. 9—The cross section of 2024 alloy weld metal made at 15 Hz laser pulse frequency showing primary dendrite arm spacing.

Moreover, to confirm the validation of the thermal model predictions, including thermal gradient ($\frac{\partial T}{\partial x}$) and cooling rate ($\frac{\partial T}{\partial t}$), the actual primary dendrite arm spacing in 2024 alloy, obtained from SEM images of 2024 alloy weld zone, was compared to that predicted by simulation using Hunt's model.^[2] This model proposes that primary dendrite arm spacing can be predicted using Eq. [11].

$$\lambda_1 = C \times \left(\frac{\partial T}{\partial x} \right)^{-0.25} \times \left(\frac{\partial T}{\partial t} \right)^{-0.25} \quad [11]$$

For Al-Cu alloys, C is^[2] given by

$$C = 0.00065 \text{ m}^{0.75} \text{ K}^{0.5} \text{ s}^{-0.25}$$

Metallographic study of the samples showed that the primary dendrite arm spacing of 2024 alloy-welded sample made at 15 Hz was 2.5×10^{-6} m (see Figure 9). The predicted primary dendrite arm spacing with regard to the calculated $\frac{\partial T}{\partial t}$ (24×10^3 K/s) and $\frac{\partial T}{\partial x}$ (4×10^5 K/m) was 2×10^{-6} m, supporting a reasonable accuracy for the simulation process.

For simplicity, the average weld pool temperature (T_a) was used for the calculation of Mg evaporation flux. The average temperature can be estimated by

$$T_a = \frac{\int_{t_s}^{t_f} T(t) dt}{t_f - t_s} \quad [12]$$

In this equation, t_s is the time when the liquid starts to form and t_f is solidification finish time. It is assumed that the liquid in the weld pool behaves as a regular solution.^[7] In a regular solution, the activity coefficients of Mg at different temperatures can be related to each other by^[10]

$$\ln \gamma_{\text{Mg}} \text{ at } T_1 = \frac{T_2}{T_1} \ln \gamma_{\text{Mg}} \text{ at } T_2 \quad [13]$$

The activity coefficients of Mg at the temperature of 1703 K (1430 °C) is equal to 0.23.^[7]

The calculation of Mg evaporation in terms of mass per unit area is shown in Figure 10, indicating that the loss was decreased by increasing the laser pulse frequency. The model shows that this decrease in Mg evaporation was mainly due to a decrease in the effective melt temperature as the pulse energies were decreased by increasing the pulse frequency (see Figure 10). However, the calculations and actual chemical analysis results of the weld metals of alloys 5083 and 5456 showed that Mg concentration in the weld metals was decreased by increasing the laser pulse frequency. This apparent contradiction can be explained by taking into account some other factors determining the Mg concentration in the final weld metal. With the increasing laser pulse frequency (at fixed average power, *i.e.*, decreasing pulse energy), the penetration or the volume of the weld pool decreased. Lower volume of the weld pool (a shallower weld) made smaller loss of Mg per unit area even more effective in the Mg loss in terms of concentration in the weld pool (per volume). In contrast to the increase in the laser pulse frequency, there were multiple Mg evaporations and according to Eqs. [6] and [7], the Mg concentration of the weld pool decreased at the initiation of subsequent melting cycles. Accordingly, the increase in overlapping could contribute to a reduction in final Mg concentration.

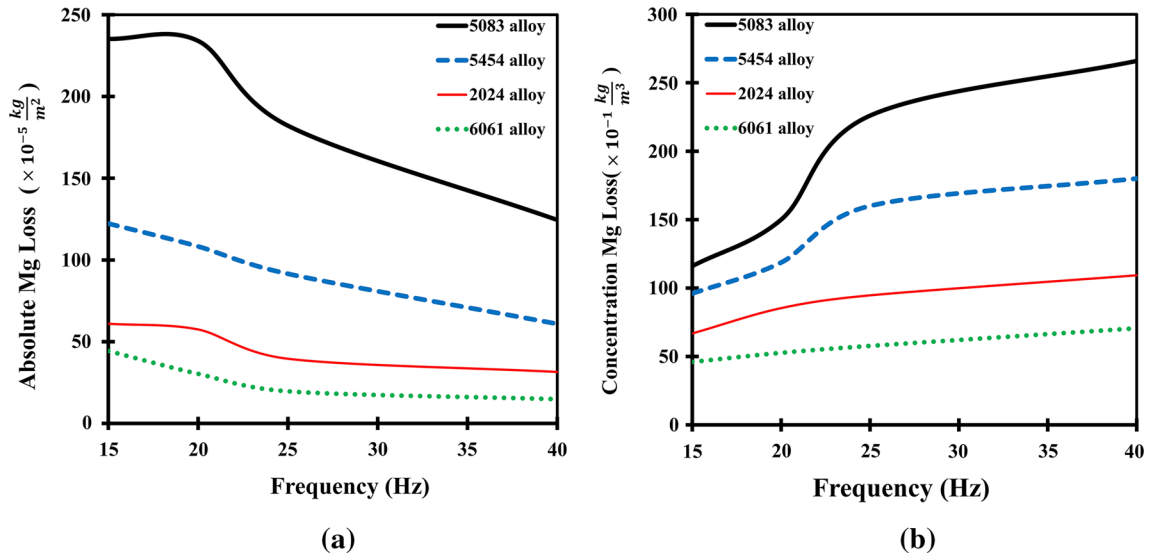


Fig. 10—Calculated Mg evaporation and the effect on Mg concentration of the weld metal in pulsed laser welding of Al alloys. (a) Mg evaporation per unit surface area of weld and (b) Mg concentration loss in the final weld metal.

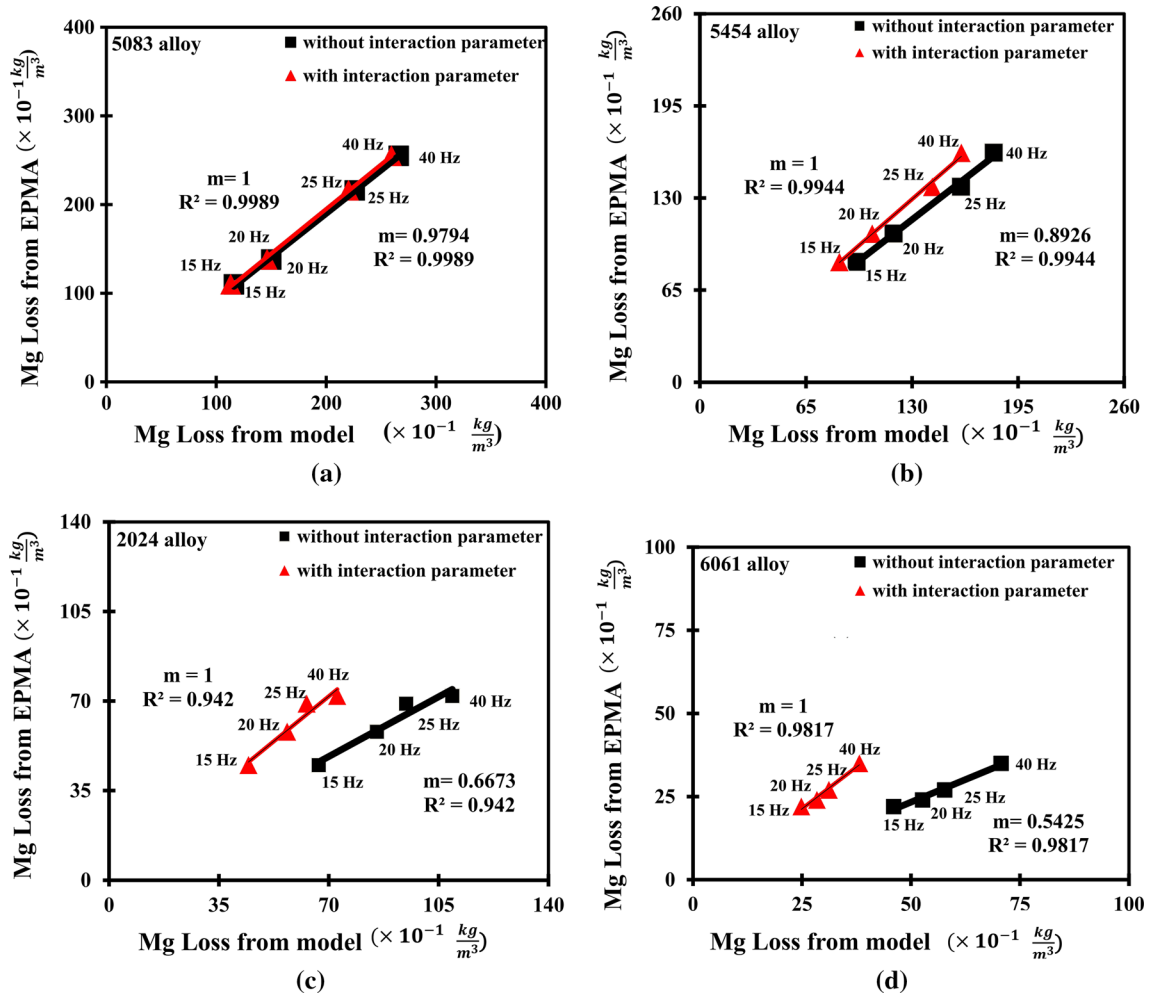


Fig. 11—The correlation of the weld metal Mg loss using EPMA analysis and evaporation model with and without correction for interaction effects. (a) 5083 alloy, (b) 5454 alloy, (c) 2024 alloy, and (d) 6061 alloy.

The comparison between the computational and experimental measurements is presented in Figure 11. Note that the lines drawn without any modification are black lines. Here, “ m ” represents the slope of the best fit and “ R^2 ” represent the correlation factor. For having a high correlation, one may expect both “ m ” and “ R^2 ” to be close to 1.

It can be seen that R^2 values for alloys containing higher Mg content (5454 and 5083) were just over 0.99. However, for other alloys, significant deviation existed. This deviation can be due to the interaction between Mg and other elements. The presence of other alloying elements in the solution changed the activity coefficient of Mg from f_{Mg}^{Mg} to f_{Mg} . The activity coefficient was affected by the concentration of alloying elements according to the following equation:

$$\begin{aligned} \text{Log } f_{Mg} = & \left(e_{Mg}^{Mg} \times \text{wt pct}_{Mg} \right) + \left(e_{Mg}^{Mn} \times \text{wt pct}_{Mn} \right) \\ & + \left(e_{Mg}^{Si} \times \text{wt pct}_{Si} \right) + \left(e_{Mg}^{Cu} \times \text{wt pct}_{Cu} \right). \end{aligned} \quad [14]$$

In the above equation, (e_j^i) is the interaction parameter of i on j . In order to estimate f_{Mg} , the gradient line of the experimental results was studied. Accordingly, the effective values of f_{Mg} for alloys 5083, 5454, 2024, and 6061 were estimated as 0.224, 0.214, 0.175, and 0.155, respectively. Considering the fact that e_{Mg}^{Mg} is 1, Eq. [13] can be written for each of the actual compositions of alloys 5454, 2024, and 6061. By solving the equations, the values of the three unknown factors (e_{Mg}^{Mn}) , (e_{Mg}^{Si}) , and (e_{Mg}^{Cu}) were calculated as -0.712 , -1.187 , and -0.032 , respectively. Here, the data on the fourth alloy could be used to check the relative accuracy of the approach. The calculated coefficients were inserted in Eq. [13] for various concentrations of the alloy 5083, and the computed activity coefficient of Mg (f_{Mg}) was found to be 0.217. On the other hand, as discussed earlier, the experimental results revealed a value of 0.224 for the activity coefficient of Mg in alloy 5083, indicating that under the given circumstances, a relative accuracy of about 97 pct existed. It must be noted that the above relations regarding activity coefficient assumed an equilibrium condition. Thus, the approach taken was a true simplification of the ultrafast heating and cooling rates involved in pulsed laser welding.

IV. CONCLUSION

An analytical model was developed in order to calculate the Mg evaporation in Nd:YAG pulsed laser welding of Al alloys in conduction mode. The weld pool temperature, Mg vapor pressure, and multiple evaporations in overlapping laser pulses were considered the primary factors controlling the Mg evaporation from the weld pool in the proposed model. The validity of the model was investigated by the experiments involving

laser welding of 2-mm-thick sheets of four Al alloys (5083, 5454, 6061, and 2424) with the variation of laser frequency (15 to 40 Hz). The average power was fixed at 200 W, and the elemental analysis of weld pools was carried out by EPMA method. The most important findings are as follows:

1. The best quantitative correlation was found between the model and experimental results regarding Mg evaporation for alloy 5083 containing the highest Mg concentration of Mg at 4.3 wt pct.
2. The model demonstrated that the absolute loss of Mg for alloy 5083 decreased from 230×10^{-5} to 120×10^{-5} kg/m² with the increasing laser pulse frequency in the range from 15 to 40 Hz due to the reduction in the average weld pool temperature in the range from 1693 K to 1613 K (1420 °C to 1340 °C). However, calculated results simultaneously demonstrated that the loss of Mg concentration in the weld metal for 5083 alloy increased from 11×10^{-1} to $28,226 \times 10^{-1}$ kg/m³ due to the reduction in the weld pool volume and multiple evaporations in the overlapping of laser pulses that occurred with the increasing pulse frequency.
3. The initial Mg content of the base metal and other alloying elements played an important role in the Mg activity and thereby in the Mg evaporation.
4. For alloys with less Mg content and higher amounts of Si, Cu, and Mn (5454, 6061, and 2024), the Mg evaporation rates decreased because of the interaction between Mg and other elements. However, the model can still predict the Mg loss trend, and the effects observed in the model can be justified by incorporating the correction factor into the activity coefficients.

REFERENCES

1. M. Sheikhi, F. Malek Ghaini, and H. Assadi: *Acta Mater.*, 2015, vol. 82, pp. 491–502.
2. E.J. Michaud, H.W. Kerr, D.C. Weckman: *Trend in Welding Research, Proceeding of the 4th International Conference*, 1995, pp. 153–58.
3. J. Liu and S. Kou: *Acta Mater.*, 2015, vol. 100, pp. 359–68.
4. X. He, T. DebRoy, and P.W. Fuerschbach: *J. Phys. D Appl. Phys.*, 2003, vol. 36, pp. 3079–88.
5. T.Y. Kuo and H.C. Lin: *Mater. Sci. Eng. A*, 2006, vol. 416, pp. 281–89.
6. H. Zhao, D.R. White, and T. DebRoy: *Int. Mater. Rev.*, 1999, vol. 44, pp. 238–66.
7. M.J. Creslak and P.W. Fuerschbach: *Metall. Trans. B*, 1988, vol. 19B, pp. 319–29.
8. J.M. Sánchez-Amaya, T.D. Pérez, J. de Damborenea J. Botana: *Sci. Technol. Weld. Join.*, 2009, vol. 14, pp. 78–86.
9. F. Tenner, Ch. Brock, F. Gürtler, F. Klämpfl, and M. Schmidt: *Phys. Proc.*, 2014, vol. 56, pp. 1268–76.
10. C.B. Miller: *Laser Welding Article*, Laser Corporation, Wyckoff, 2016.
11. D.W. Moon and E.A. Metzbower: *Weld. Res. Suppl. J*, 1983, vol. 62, pp. 53–58.
12. J.P. Weston, I.A. Jones, and E.R. Wallach: *6th International Conference on Welding and Melting by Electron and Laser Beams*. 1998.

13. X. He, T. DebRoy, and P.W. Fuerschbach: *J. Phys. D Appl. Phys.*, 2004, vol. 96, pp. 4547–55.
14. U. Dilthey, A. Goumeniouk, V. Lopota, G. Turichin, and E. Valdaitseva: *J. Phys. D Appl. Phys.*, 2001, vol. 34, pp. 81–86.
15. R. Rai, S.M. Kelly, R.P. Martukanitz, and T. Debroy: *Metall. Trans. A*, 2008, vol. 39A, pp. 98–112.
16. T. Mukherjee, J.S. Zuback, A. De, and T. DebRoy: *Sci. Rep.*, 2016, vol. 6, pp. 1–6.
17. A. Block-Bolten and T.W. Eagar: *Metall. Trans. B*, 1984, vol. 15B, p. 461.
18. P. Parvin and M.J. Torkamany: *J. Phys. D Appl. Phys.*, 2009, vol. 42, pp. 1–8.
19. D.R. Gaskell: *Introduction to the Thermodynamics of Materials*, 5th ed., CRC Press, Boca Raton, 2008, pp. 66–91.
20. C.L. Young, R. Battino, & H. L. Clever: in *Solubility Data Series V7*, R. Battino, ed. Pergamon Press, Oxford, 1981, pp. 15–20.
21. X. He, T. DebRoy, and P.W. Fuerschbach: *J. Phys. D Appl. Phys.*, 2004, vol. 6, pp. 4547–55.
22. N. Ahmed: *New Developments in Advanced Welding*, Woodhead Publishing Ltd, New York, 2005, pp. 115–16.
23. M.R. Frewin and D.A. Scott: *Weld. J.*, 1999, vol. 15, pp. 15–22.
24. A. De, C.A. Walsh, S.K. Maiti, and H.K.D.H. Bhadeshia: *Sci. Technol. Weld. Joining*, 2003, vol. 8, pp. 391–99.
25. S. Bag, A. Trivedi, and A. De: *Int. J. Therm. Sci.*, 2009, vol. 48, pp. 1923–31.
26. T. Bergman, A. Lavine, F. Incropera, and D. DeWitt: *Fundamentals of Heat and Mass Transfer*, 5th ed., Wiley, New York, 2008, pp. 268–324.
27. S. Bag and A. De: in: *Laser Welding*, X. Na, ed., Intech, 2010, pp. 133–60.
28. N. Zhao, Y. Yang, M. Han, X. Luo, G. Feng, and R. Zhang: *Trans. Nonferrous Met. Soc. China*, 2012, vol. 22, p. 2226.
29. D.C. Weckman, H.W. Kerr, and J.T. Liu: *Metall. Trans. B*, 1997, vol. 28B, pp. 687–700.
30. M. Zain-ul-abdein, D. Nelias, J. Jullien, and D. Deloison: *Mater. Sci. Eng.*, 2010, vol. 527, pp. 3025–39.